J Mater Sci: Mater Electron (2015) 26:6563–6571
DOI 10.1007/s10854-015-3254-2

Synthesis of novel *s*-triazine/carbazole based bipolar molecules and their application in phosphorescent OLEDs

Tianxing Lu[1,2] · Jing You[1,2] · Dan Zhao[3] · Hua Wang[3] · Yanqin Miao[3] · Xicheng Liu[1,2] · Yin Xiao[1,2] · Xianggao Li[1,2] · Shirong Wang[1,2]

Received: 13 January 2015 / Accepted: 24 May 2015 / Published online: 5 June 2015

Abstract Three *s*-triazine/carbazole based bipolar molecules: 9,9′,9″-(1,3,5-triazine-2,4,6-triyl)tris(3,6-di-*tert*-butyl-carbazole) (TazTCz), 9,9′-(6-phenyl-1,3,5-triazine-2,4-diyl) bis(3,6-di-*tert*-butyl-carbazole) (PhTazDCz) and 9-(4,6-diphenyl-1,3,5-triazine-2-yl)-3,6-di-*tert*-butyl-carbazole (DPhTazCz) were synthesized and applied as host materials for blue phosphorescent organic light-emitting diodes (PHOLEDs). The triplet state energy levels are ~2.86 eV for these compounds, ensured their application in blue PHOLEDs. X-ray single crystal structural analysis revealed a non-planar structure of TazTCz, which prevented the intermolecular close-packing in the solid state. X-ray diffraction spectra also confirmed that TazTCz and PhTazDCz could form amorphous films with spin-coating method. The bipolar characteristics of as-synthesized compounds were confirmed by carrier mobility measurement. The device parameters of blue PHOLEDs based on these compounds as host materials exhibit that the balance of electron and hole mobilities is benefit for reducing turn-on voltage and efficiency roll-off at high current density.

✉ Jing You
Youj1983@tju.edu.cn

[1] Department of Applied Chemistry, School of Chemical Engineering and Technology, Tianjin University, Tianjin 300072, China

[2] Collaborative Innovation Center of Chemical Science and Engineering, Tianjin 300072, China

[3] Key Laboratory of Interface Science and Engineering in Advanced Materials, Taiyuan University of Technology, Ministry of Education, No. 79 Yingze Street, Taiyuan 030024, Shanxi, China

1 Introduction

In the past decades, organic light-emitting diodes (OLEDs) have tremendous development in fields of flat-panel displays and solid state lighting [1–4]. Carrier recombination is expected to form triplet and singlet excitons in a ratio of 3:1 under the electric field [5]. In theory, the internal quantum efficiency can approach to 100 % by utilizing both triplet and singlet excitons in phosphorescent OLEDs (PHOLEDs) [6]. Generally, the host–guest structure of emitting layer is adopted to suppress concentration quenching and triplet–triplet annihilation.

Charge recombination zone is considered to be one of most important factors for highly efficient PHOLEDs. The narrow recombination zone has negative effect on the operation stability due to the triplet–triplet annihilation [7]. One strategy is using bipolar host materials comprising of electron-donating and electron-withdrawing moieties in one molecule [8, 9]. In addition, the host materials also require high thermal stability, suitable energy levels, especially for the triplet state.

4,4′-bis (9-carbazolyl) biphenyl (CBP) as one of the most widely used phosphorescent host materials has high hole mobility because of the carbazolyls in CBP [10]. However, the glass transition temperature (T_g) of CBP is only 62 °C. Namely, the CBP is very easy to form crystal in the films [11]. Moreover, the low triplet state energy level (E_T ~ 2.56 eV) limits its application in the blue PHOLEDs. Therefore, it is important to develop the host materials with relatively high T_g and suitable E_T based on carbazolyl for blue PHOLEDs [12, 13]. On the other hand, the compound with *s*-triazine unit has higher electron mobility than the conventional electron transporting material 1,3,5-tris(N-phenylbenzimidizol-2-yl)benzene (TPBi) [14–16].

In this work, a serials of new phosphorescent host materials containing hole-transporting carbazole as a donor (D) and electron-transporting *s*-triazine as an acceptor (A) were successfully synthesized through nucleophilic substitution of the chlorides and organolithium reagent. The molecular structures were characterized with ^{1}H NMR, IR and mass spectra. The synthetic routes and molecular structures are shown in Scheme 1. Two *tert*-butyl groups are introduced in the 3- and 6- positions of cabarzolyl to improve the solubility in organic solvents and electrochemical reversibility of the compounds [17–19]. The effect of different phenyl/carbazolyl ratio on photoelectric properties, film morphologies and mobilities of the compounds is discussed in detail.

2 Experimental

2.1 Materials

Iodine (I_2, 99.99 %) and 2-chloro-2-methylpropane ($C(CH_3)_3Cl$, AR) were purchased from Tianjin Guangfu Fine Chemical Research Institute (Tianjin, China). Cyanuric chloride ($(NCCl)_3$, 99 %), zinc chloride ($ZnCl_2$, AR), nitromethane (CH_3NO_2, AR), n-butyllithium/hexane solution (n-BuLi, 1.6 M) and terakis(triphenylphosphine)palladium(0) ($Pd[P(C_6H_5)_3]_4$, Pd $\geq$ 9.0 %) were purchased from Aladdin Industrial Corporation (Shanghai, China). Other reagents were purchased from Tianjin Jiangtian Chemical Technology Co., Ltd. (Tianjin, China). Tetrahydrofuran (THF) was distilled before use. All the other agents were used without further treatment.

2.2 Measurement

^{1}H NMR (400 MHZ) spectra were recorded with a Bruker ACF400 (400 MHz) supplied by Bruker Biospin (Fällanden) in $CDCl_3$ with tetramethylsilane as reference. High resolution mass spectra (HRMS) were recorded on a Bruker micrOTOF-Q II (Bruker). FT-IR spectroscopy measurement was performed on a Thermo Nicolet 380 (Thermo Nicolet). UV spectra of solutions and films were recorded on a Thermo Evolution 300 UV–Vis Spectrometer (Thermo Electron). Fluorescence spectra were recorded on a F-4500 fluorescence spectrophotometer (Hitachi). Phosphorescence spectra in the solid state were recorded on a Fluorolog R5509 fluorescence spectrophotometer (Horiba) at 77 K. Thermogravimetric analysis (TGA) were performed on a TA Q500 Thermogravimetric Analyzer (TA-Instruments) with heating rate of 10 °C min^{-1} under nitrogen atmosphere. XRD spectra were recorded on a Miniflex 600 (Rigaku) with 2θ range of 2°–40°, and scanning rate of 1° per min.

The cyclic voltammetry (CV) measurement was performed on a CHI600E electrochemistry workstation with a three-electrode cell in dry dichloromethane, with the tetrabutylammonium hexafluorophosphate (n-Bu_4NPF_6, 0.1 M) as supporting electrolyte, a scanning rate of 100 mV s^{-1}. A glass carbon, a platinum wire and an $Ag/AgNO_3$ electrode were used as the working, counter and reference electrode, respectively.

X-ray crystallography of TazTCz were record with the graphine monochromated Mo Kα radiation ($\lambda = 0.71073$ Å) on a Bruker P4 four-circle diffractometer. The structure was solved with a SHELXS-97 program [20]. The non-hydrogen atoms were located in successive difference Fourier

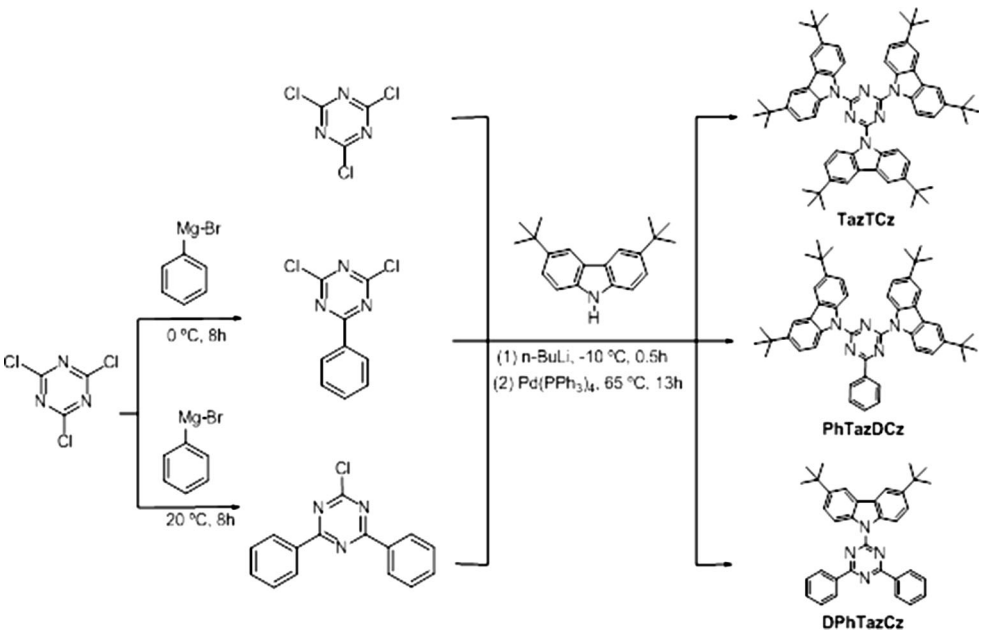

Scheme 1 Synthetic routes and molecular structures

syntheses. The final refinement was performed by full matrix least-squares methods with anisotropic parameters for non-hydrogen atoms on F^2 using the SHELXTL and OLEX2 softwares [20, 21]. Crystallographic data reported in this paper had been deposited with the Cambridge Crystal Data Centre and CCDC No. 1030490.

The time-of-flight (TOF) measurement was record on a TOF401 (Sumitomo Heavy Industries. Ltd., Japan). Samples were prepared through vacuum deposition with a structure of ITO/as-synthesized compounds ($\sim$1 μm)/Al (100 nm) with a working area of 3 × 10 mm^2. The hole or electron mobility (μ) was calculated with the equation of $\mu = d^2 \cdot V^{-1} \cdot t_\tau^{-1}$, where d, V and t_τ is film thickness, applied bias voltage and transit time, respectively.

2.3 Quantum chemical calculation

Quantum chemical calculation was performed on a Gaussian 03 program with the Beck's three-parameter exchange functional and the Lee–Yang–Parr's correlation functional (B3LYP) using 6-31G(d) basis sets [22]. The ground geometries were fully optimized and these optimized stationary points were further characterized by harmonic vibration frequency analysis to ensure that real local minima had been found. Singlet state transition energies were calculated by time-dependent density functional theory (TD-DFT) at the B3LYP/6-31G (d) level.

2.4 Fabrication of PHOLEDs

All devices were fabricated by vacuum deposition on a prepatterned indium tin oxide (ITO) glass substrate with a sheet resistance of 15 Ω sq^{-1}. The ITO substrates used as the anode were scrubbed and sonicated consecutively with detergent water, deionized water, and acetone. They were then dried in a drying cabinet and exposed to a UV–ozone environment for 10 min. The substrates were then transferred into a vacuum chamber for the sequential deposition of the organic functional layers by thermal evaporation under a vacuum of 5 × 10^{-4} Pa. The deposition rates for the organic materials, molybdenum trioxide (MoO_3), lithium fluoride (LiF) and Al were about 1, 0.3, 0.1 and 3 Å s^{-1}, respectively. The thickness and deposition rates of the films were controlled by a quartz thickness monitor. The overlap between the ITO anode and the Al cathode was 3 mm × 3 mm and formed the active emissive area of the devices. The performance of the devices was characterized with a PR655.

Spectrascan spectrometer and a Keithley 2400 programmable voltage current source. All the samples were measured directly after fabrication (without encapsulation) in an ambient atmosphere at room temperature in a darkroom.

2.5 Synthesis and characterizations

2.5.1 Synthesis of 3,6-di-tert-butyl-carbazole [23]

Carbazole (10.00 g, 59.80 mmol), $ZnCl_2$ (24.45 g, 179.41 mmol) and nitromethane (CH_3NO_2 100 ml) were added to a three-neck flask under nitrogen (N_2) atmosphere. 2-chloro-2-methylpropane (19.77 ml, 179.41 mmol) was added dropwise into above flask with stirring. After stirring for 6 h at room temperature, the mixture was diluted with water (100 ml) and extracted with dichloromethane (CH_2Cl_2, 100 ml × 3). The organic layer was washed with water (100 ml), neutralized with sodium carbonate (Na_2CO_3) solution, washed with brine (NaCl) solution (100 ml), dried with magnesium sulfate ($MgSO_4$), filtered and removed of the solvent with rotary evaporation. Recrystallization from petroleum ether (PE) gave a white powder (8.05 g, 48 % yield). M.p. 228-230 °C. ^{1}H NMR (400 MHz, $CDCl_3$) δ (ppm): 8.09 (s, 2H), 7.81 (s, 1H), 7.48 (dd, J = 13.1 Hz, 6.3 Hz, 2H), 1.46 (d, J = 2.5 Hz, 18H). MS (ESI^-), found value [M–H] 278.39, calculated value [M] 279.20.

2.5.2 Synthesis of 2,4-dichloro-6-phenyl-1,3,5-triazine

A solution of bromobenzene (PhBr, 1.6 ml, 15 mmol) in anhydrous THF (8.4 mL) was added dropwise to a stirred mixture of iodine-activated magnesium (Mg, 0.44 g, 18 mmol) in anhydrous THF (2 mL) under N_2 atmosphere. In the case of a delayed start to the reaction, brief heating was carried out. After complete addition, the reaction mixture was maintained for 2 h at reflux temperature. Then cooled to room temperature to obtain the Grignard reagent. The Grignard reagent was added dropwise to a solution of $(NCCl)_3$ (1.84 g, 10 mmol) in anhydrousTHF (20 mL) with an icy bath. After stirring for 8 h at 0 °C, the mixture was poured into a 3.6 % aqueous solution of hydrochloric acid (HCl, 20 mL). The mixture was extracted with CH_2Cl_2 (50 ml × 3), dried with $MgSO_4$, filtered and removed of the solvent with rotary evaporation. The residue was purified by column chromatography to afford a white solid (1.11 g, 49 % yield). M.p. 120–121 °C. ^{1}H NMR (400 MHz, $CDCl_3$) δ (ppm): 8.51 (d, J = 7.5 Hz, 2H), 7.66 (t, J = 7.4 Hz, 1H), 7.53 (t, J = 7.7 Hz, 2H). MS ($APCI^+$), found value [M + H]$^+$ 225.99, calculated value [M] 224.99.

2.5.3 Synthesis of 2-chloro-4,6-diphenyl-1,3,5-triazine

Following the above synthesis procedure 2.5.2, 1.08 g (67 % yield) of white solid was obtained from Mg (0.54 g, 22 mmol), PhBr (2.1 ml, 20 mmol), and $(NCCl)_3$ (1.11 g, 6 mmol) at room temperature for 8 h. M.p. 140–142 °C. ^{1}H NMR (400 MHz, $CDCl_3$) δ (ppm): 8.62 (d, J = 7.5 Hz, 4H), 7.63 (t, J = 7.3 Hz, 2H), 7.55 (t, J = 7.5 Hz, 4H). MS

(APCI$^+$), found value [M + H] $^+$ 268.33, calculated value [M] 267.06.

2.5.4 Synthesis of 9,9′,9″-(1,3,5-triazine-2,4,6-triyl)tris(3,6-di-tert-butyl-carbazole) (TazTCz)

3, 6-di-*tert*-butyl-carbazole (4.47 g, 16 mmol) was placed in a 100 mL round-bottom flask equipped with a stir. Anhydrous THF (30 mL) was injected with a syringe into the flask under N_2 atmosphere. Then the solution was cooled in an ice-salt bath and 1.6 M n-BuLi/hexane solution (10 mL, 16 mmol) was added into slowly with a syringe. The mixture was stirred for another 30 min at room temperature to obtain organolithium reagent. The organolithium reagent was slowly dropped into a mixture of $(NCCl)_3$ (0.92 g, 5 mmol) and [$Pd(PPh_3)_4$] (173 mg) in anhydrous THF solution (20 mL). The reaction mixture was maintained at reflux temperature for 13 h, then cooled to room temperature. The mixture was added with water (50 ml) and extracted with CH_2Cl_2 (50 ml × 3), dried with $MgSO_4$, filtered and removed of the solvent under reduced pressure. The residue was purified by column chromatography to afford a white solid (2.38 g, 52 % yield). M.p. > 250 °C. ^{1}H NMR (400 MHz, $CDCl_3$) δ (ppm): 8.90 (d, J = 8.8 Hz, 6H), 8.11 (d, J = 1.4 Hz, 6H), 7.51 (dd, J = 8.8 Hz, 1.6 Hz, 6H), 1.51 (s, 54H). MS (APCI$^+$), found value [M + H] $^+$ 913.34, calculated value [M] 912.58. IR (KBr), ν/cm^{-1} 3051, 2958, 2868, 1628, 1585, 1539, 1489, 1460, 1412, 1296, 1271, 1252, 1209, 1167, 1103, 1034, 876, 818, 769, 737, 700, 652, 613 cm^{-1}.

2.5.5 Synthesis of 9,9′-(6-phenyl-1,3,5-triazine-2,4-diyl)bis(3,6-di-tert-butyl-carbazole) (PhTazDCz)

Following the synthesis procedure 2.5.4, 2.24 g (63 % yield) of white solid was obtained from 3,6-di-*tert*-butyl-carbazole (3.35 g, 12 mmol), 1.6 M n-BuLi/hexane solution (7.5 ml, 12 mmol), 2,4-dichloro-6-phenyl-1,3,5-triazine (1.13 g, 5 mmol), $Pd(PPh_3)_4$ (231 mg) at reflux temperature for 13 h. M.p. > 250 °C. ^{1}H NMR (400 MHz, $CDCl_3$) δ (ppm): 8.99 (H, d, J = 8.8 Hz, 4H), 8.84-8.71 (H, m, 2H), 8.13 (H, d, J = 1.6 Hz, 4H), 7.70 (H, d, J = 1.2 Hz, 2H), 7.68 (H, d, J = 8.9 Hz, 1H), 7.62 (dd, J = 8.8 Hz, 1.8 Hz, 4H), 1.54 (s, 36H). MS (APCI$^+$), found value [M + H] $^+$ 712.53, calculated value [M] 711.43. IR (KBr), ν/cm^{-1} 3064, 2958, 2868, 1630, 1587, 1535, 1485, 1464, 1443, 1406, 1298, 1257, 1213, 1171, 1099, 1032, 876, 844, 820, 773, 739, 696, 672, 652, 613 cm^{-1}.

2.5.6 Synthesis of 9-(4,6-diphenyl-1,3,5-triazine-2-yl)-3,6-di-tert-butyl-carbazole (DPhTazCz)

Following the above synthesis procedure 2.5.4, 2.66 g (52 % yield) of white solid was obtained from 3,6-di-*tert*-butyl-carbazole (2.79 g, 10 mmol), 1.6 M n-BuLi/hexane solution (6.25 ml, 10 mmol), 2-chloro-4,6-diphenyl-1,3,5-triazine(2.14 g, 8 mmol), 277 mg $Pd(PPh_3)_4$ at reflux temperature for 13 h. M.p. > 250 °C. ^{1}H NMR (400 MHz, $CDCl_3$) δ (ppm): 8.09 (s, 2H), 7.81 (s, 1H), 7.48 (m, 2H), 7.34(d, J = 8.4 Hz, 2H), 1.46 (s, 18H). MS (APCI$^+$), found value [M + H]$^+$ 511.49, calculated value [M] 510.28. IR (KBr), ν/cm^{-1} 3063, 2958, 2868, 1630, 1587, 1529,1471, 1446, 1410, 1373, 1300, 1255, 1221, 1174, 1105, 1030, 899, 872, 839, 822, 764, 742, 704, 696, 663, 652, 613 cm^{-1}.

3 Results and discussion

3.1 Spectra and energy level characteristics

The UV/Vis absorption and fluorescence spectra of TazTCz, PhTazDCz and DPhTazCz in the solid films are shown in Fig. 1. The optical energy band gaps (E_g) were calculated from the onset of absorption spectra (λ_{onset}). The triplet state energies (E_T) determined by the 0-0 transition peaks from the phosphorescence spectra are ~2.86 eV indicating good confinement of the triplet exciton on FIrpic (E_T = 2.62 eV). Electrochemical properties of as-synthesized compounds were investigated by CV measurement. Spectra and energy levels of the compounds are summarized in Table 1. As shown in Table 1 and Fig. 1, the lowest excitation energies (E_{0-0}) decrease with increasing the number of phenyl attached on the *s*-triazine.

The energy levels and the corresponding frontier orbital distributions (see Fig. 2) were calculated by DFT method. The highest occupied molecular orbital (HOMO) levels are roughly the same, while the lowest unoccupied molecular orbital (LUMO) energy levels decrease gradually with the

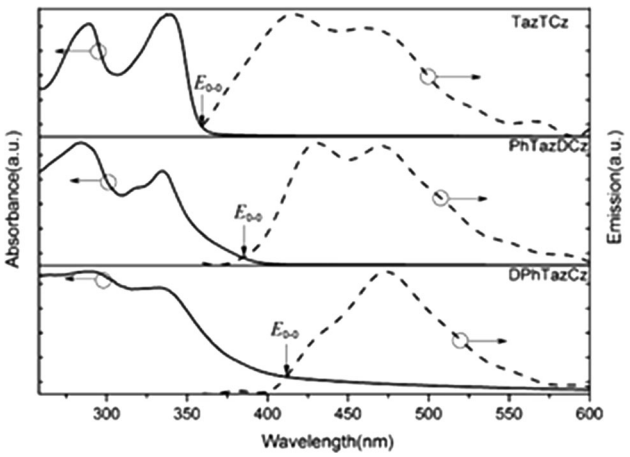

Fig. 1 The absorption spectra (*solid line*) and fluorescence spectra (*dotted line*) of solid films

Table 1 Optical and energy levels data of as-synthesized compounds

Expt.										Calcd.[g]
Compd.	λ_{onset} (nm)[a]	E_g (eV)	E^{ox}_{onset} (V)[b]	HOMO/LUMO (eV)[c]	λ^{max}_{abs} (nm)	λ^{max}_{em} (nm)	E_{0-0} (eV)[d]	E_T (eV)[e]	φ^f_f	HOMO/LUMO (eV)
TazTCz	357	3.47	1.21	−5.85/−2.38	289/337	416/462	3.45	2.86	0.28	−5.52/−1.20
PhTazDCz	390	3.18	1.21	−5.85/−2.67	284/335	430/470	3.22	2.86	0.36	−5.56/−1.70
DPhTazCz	407	3.05	1.25	−5.89/−2.84	292/332	474	3.02	2.84	0.44	−5.57/−1.84

[a] Determined from absorption spectra of the solid films

[b] The onset potentials of oxidation determined from CV measurement

[c] $E_{HOMO} = -(E^{ox}_{onset} - E_{FC/FC^+}) - 4.8$. $E_{LUMO} = E_{HOMO} + E_g$

[d] The lowest excitation energy determined from the intersection point of absorption and emission spectra

[e] The triplet state energies (E_T) determined by the 0–0 transition peaks from the phosphorescence spectra

[f] The fluorescence quantum yields calculated as referenced to quinine sulfate [24]

[g] Calculated at the B3LYP/6-31G (d) level

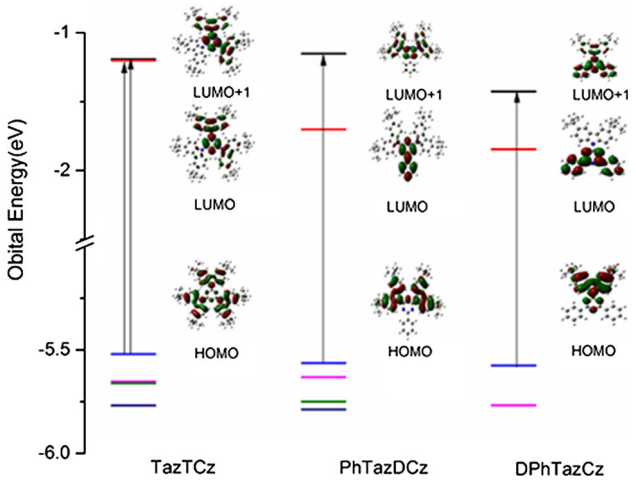

Fig. 2 The energy levels and the corresponding frontier orbital distributions obtained by quantum chemical calculation

increase of phenyl attached on the *s*-triazine. These results agree with the tendency determined by electrochemical measurement.

The fluorescence quantum yields of TazTCz, PhTazDCz and DPhTazCz in the solutions of toluene increased from 0.28 to 0.44 with replacing carbazolyl by phenyl (see Table 1). From the optimized ground state structures, the dihedral angles between *s*-triazine and carbazolyl are >17°, whereas the dihedral angles between *s*-triazine and phenyl are <13° (see Table 2). Therefore, the overall planarity of molecule and conjugation degree can be increased with increasing the number of phenyl attached on the *s*-triazine, resulting in the red-shifted emission peaks and the improvement of the fluorescence quantum yield. Moreover, the molecular symmetry of PhTazDCz (C_2) and DPhTazCz (C_2) is also reduced compared with TazTCz (C_3). Correspondingly, the molecule dipole moment (μ) increases

Table 2 The dihedral angles and dipole moments from the optimized ground state structures

Compd.	∠Cz − Taz (degree)[a]	∠PhTaz (degree)[b]	μ (D)
TazTCz	20.59/20.60/20.82	–	0.06
PhTazDCz	18.95/19.04	12.88	0.31
DPhTazCz	17.24	9.39/9.39	0.38

[a] The dihedral angles between carbazolyl moiety and *s*-triazine moiety

[b] The dihedral angles between phenyl moiety and *s*-triazine moiety

from 0.06 D for TazTCz to 0.38 D for DPhTazCz (see Table 2).

The vertical electronic transitions were calculated by TD-DFT method at the B3LYP/6-31G (d) level. It shows the maximum absorption peak at 332 nm of TazTCz mainly originates from the transitions of HOMO → LUMO (73 %) and HOMO → LUMO + 1 (73 %). However, the HOMO → LUMO transitions are forbidden for PhTazDCz and DPhTazCz due to the lack of spatial overlap between the HOMO and LUMO orbitals (see Fig. 2). Accordingly, the absorption peak at 326 nm for PhTazDCz mainly originates from the transition of HOMO → LUMO + 1 (93 %) and the absorption peak at 335 nm for DPhTazCz originates from the transition of HOMO → LUMO + 1 (90 %). As to absorption spectra (see Fig. 1), all of these three as-synthesized compounds show a strong peak in the region 330–350 nm.

3.2 Crystal structure of TazTCz

A colorless bulk crystal of TazTCz was obtained by crystallization from toluene and acetonitrile solution. The propeller-shaped single crystal structure and intermolecular

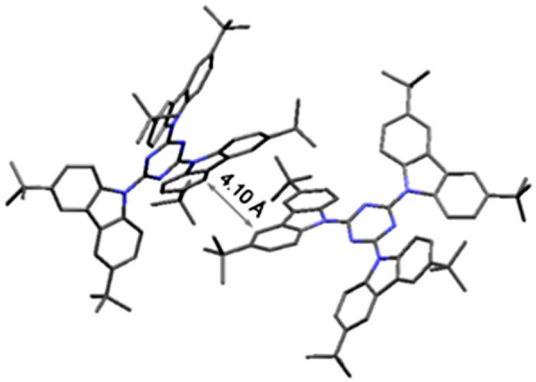

Fig. 3 The propeller-shaped single crystal structure and intermolecular crystal stacking structure of TazTCz

crystal stacking structure of TazTCz are showed in Fig. 3, hydrogen atoms are omitted for clarity.

The dihedral angles between carbazolyl and *s*-triazine are 22.66°, 22.72° and 26.84°, respectively, corresponding to the quantum chemical calculation (see Table 2). The propeller-shaped non-planar structure impedes the intermolecular close-packing in solid state. The intermolecular crystal packing indicates the absence of intermolecular π–π interaction, in which the closest point-to-point distance between carbazolyl moieties is 4.10 Å. This large intermolecular separation results from the twisted molecule conformation and a steric effect of the substituted *tert*-butyl.

3.3 Thermal analysis and the amorphousness of films

The TGA measurement exhibits the 5 % weight loss temperatures of TazTCz, PhTazDCz and DPhTazCz at 462, 384 and 341 °C, respectively. The good thermal properties of these compounds are suitable for both thermal evaporation and device operation.

The crystallization properties of the solid films fabricated with spin-coating were estimated from X-ray diffraction (XRD) spectra (see Fig. 4). The XRD spectra show featureless broad shape in the spectra of TazTCz and PhTazDCz, which indicate the amorphous nature of thin films suitable for wet-processing fabrication. A sharp diffraction peak in the XRD spectrum of DPhTazCz indicates the crystallization of thin film.

3.4 Carrier mobility and phosphorescent organic light-emitting diodes

The carrier mobility of as-synthesized compounds was evaluated with the time-of-flight (TOF) method. The electron and hole mobilities of as-synthesized compounds at $\sim 2 \times 10^5$ V cm^{-1} are summarized in Table 3. Electron mobilities are in the range of 1.46×10^{-6}–5.83×10^{-6}

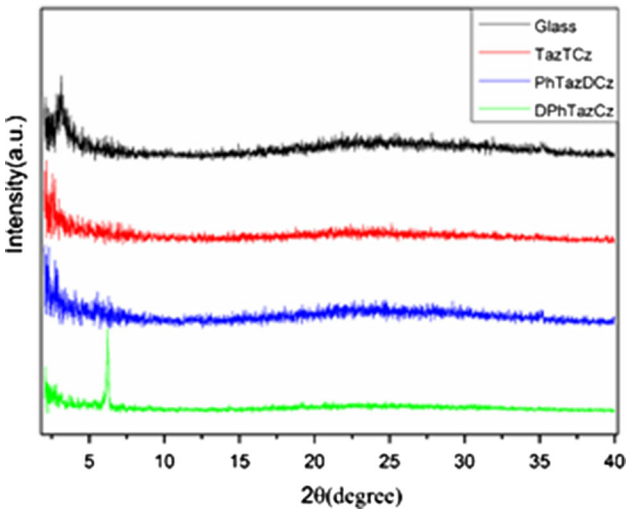

Fig. 4 X-ray diffraction spectra of the thin film samples on glass substrates

cm^2 V^{-1} s^{-1}. There is no obvious variation though replacing carbazolyl with phenyl. However, the variation of hole mobility is obvious. As shown in Table 3, the hole mobility of TazTCz is 10 times larger than that of DPhTazCz. It was reported that the increase in the dipole moment could reduce the hole mobility of the donor compound [25]. As discussed above, after replacing carbazolyl with phenyl, it changes into a polar molecule DPhTazCz ($\mu = 0.38$ D) from a nonpolar molecule TazTCz ($\mu = 0.061$ D) leading to a decrease of hole mobility. Compared PhTazDCz with DPhTazCz, the molecular dipole moments are roughly same. Therefore, the hole mobilities are in the same order of magnitude.

The PHOLEDs were fabricated with TazTCz, PhTazDCz and DPhTazCz as host materials. The schematic structure, an energy level diagram of the device and the molecular structure of the materials used in the devices are shown in Fig. 5a–c, respectively. The electroluminescence (EL) spectra of PHOLEDs with TazTCz as host at different current densities are shown in Fig. 5d.

Here, MoO_3 and LiF are used as hole and electron injection layers, respectively. N,N'-bis(naphthylphenyl)-4,4′-biphenyldiamine (NPB) and 1,3,5-tris(N-phenylbenzimidizol-2-yl)benzene (TPBi) are used as hole transporting and electron transporting layers, respectively. Di-[4-(N, N-ditolyl-amino)-phenyl] cyclohexane (TAPC) is employed as exciton-blocking layer. Iridium (III) bis [(4, 6-di-fluorophenyl)-pyridinato-N, $C^{2\prime}$] picolinate (FIrpic) is served as the blue-emitting phosphor. TazTCz, PhTazDCz and DPhTazCz synthesized in this work are applied as host materials in the emitting layer.

The PHOLEDs exhibit a stable emission peak around 472 nm and a shoulder at 500 nm at different current densities, which are from the emission of FIrpic (Fig. 5d).

Table 3 The electron and hole mobilities of host at $\sim 2 \times 10^5$ V cm^{-1} and the device parameters

Host	Electron (cm^2 V^{-1} s^{-1})	Hole (cm^2 V^{-1} s^{-1})	$V_{turn\text{-}on}$ (V)	L_{max} (cd m^{-2})[a]	η_{max} (cd A^{-1})[b]	η_{10} (cd A^{-1})[c]	η_{100} (cd A^{-1})[d]
TazTCz	5.83×10^{-6}	1.20×10^{-5}	4.14	1185	2.46	2.37	1.14
PhTazDCz	4.22×10^{-6}	4.54×10^{-6}	2.78	1961	0.82	0.78	0.72
DPhTazCz	1.46×10^{-6}	1.04×10^{-6}	4.00	2380	0.97	0.86	0.74

[a] Maximum luminance

[b] Maximum current efficiency

[c] The current efficiency at 10 mA cm^{-2}

[d] The current efficiency at 100 mA cm^{-2}

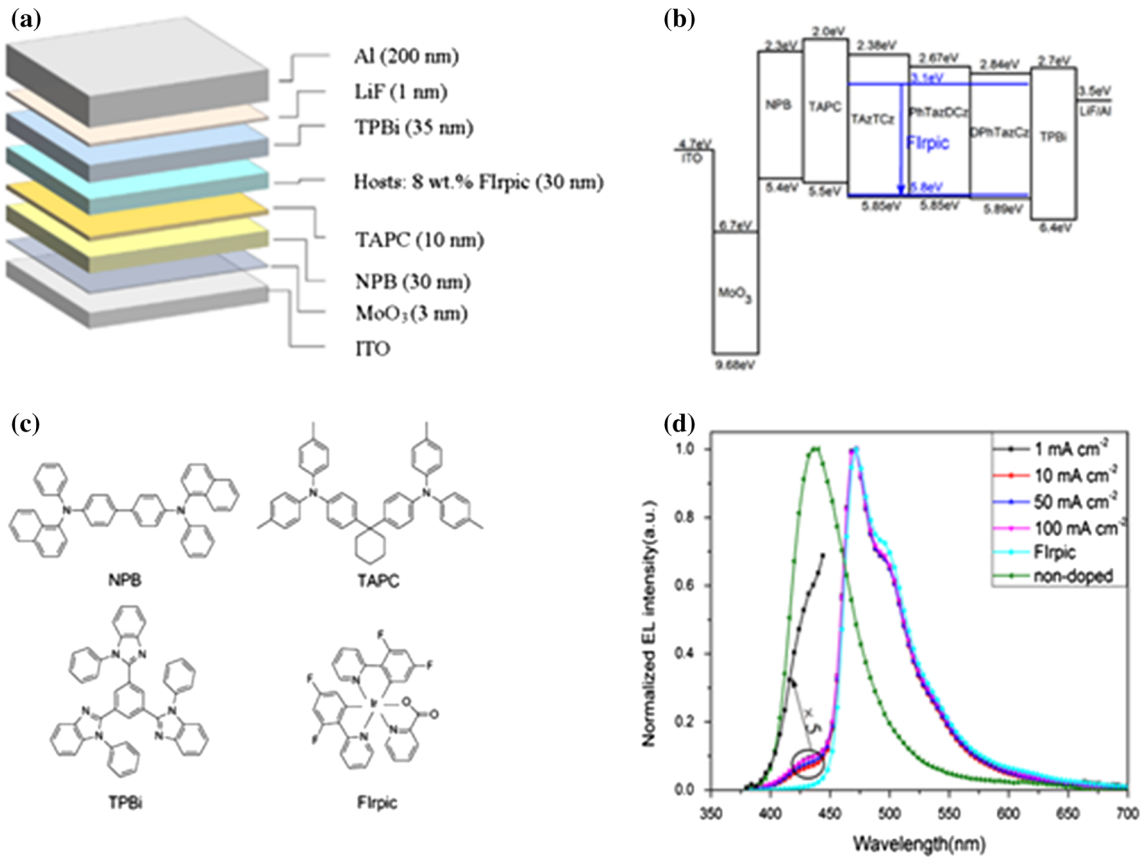

Fig. 5 The schematic structure (**a**) and an energy level diagram (**b**) of devices. The molecular structure of the materials (**c**) used in the devices. The EL spectra (**d**) of PHOLEDs with TazTCz as host at different current densities

However, the EL spectra of PHOLED with TazTCz as host show a new peak in 400–450 nm region (Fig. 5d black dotted line). It can be confirmed that the new peak generates from the emission of TazTCz by comparing with the EL spectrum of non-doped PHOLED with TazTCz as the emitting layer. From the energy level diagram in Fig. 5b, the HOMO energy levels of TazTCz and FIrpic are too close, which cause the incomplete energy transfer from TazTCz to FIrpic.

The device parameters of PHOLEDs are shown in Table 3. The current density–voltage-luminance (*J*–*V*–*L*) characteristics and the current efficiency-current density curves of devices are shown in Fig. 6a, b respectively. The turn-on voltage (defined as the voltage at 1 cd m^{-2}) of PHOLED with PhTazDCz as host is lower than that of the PHOLEDs with DPhTazCz and TazTCz as hosts. The values of the energy barrier are determined by the LUMO energy level differences between 1,3,5-tris(N-phenylbenzimidizol-2-yl)benzene (TPBi) and the hosts, which are 0.32, 0.03 and 0.14 eV for the PHOLEDs with TazTCz, PhTazDCz and DPhTazCz as hosts (see Fig. 5b), respectively. Therefore, these results suggest that the lower electron injection energy barrier from the electron

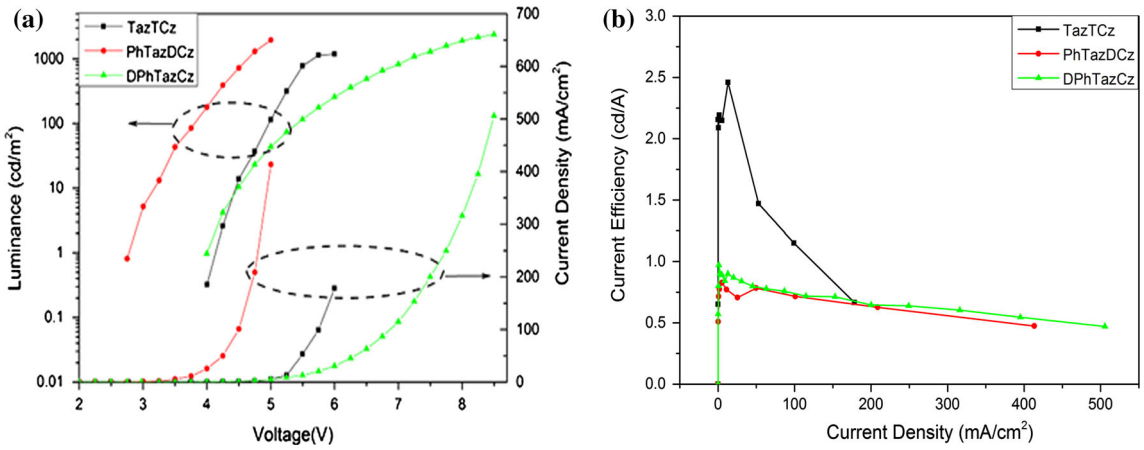

Fig. 6 *J–V–L* characteristic curves (**a**) and the current efficiency-current density curves (**b**) of devices

transporting layer to the emissive layer leads to the lower turn-on voltage of PHOLEDs.

As shown in Fig. 6b, the efficiency roll-off at high current density of PHOLEDs with PhTazDCz and DPhTazCz as hosts is reduced through increasing the balance of electron and hole mobilities of PhTazDCz and DPhTazCz (see Table 3). This balance could distribute excitons evenly in the emitting layer, which is favorable for exciton formation and light emission. It indicates that the introduction of phenyl around the *s*-triazine could improve the energy transfer efficiency from host materials to FIrpic and balance carrier mobilities.

4 Conclusions

Three bipolar small molecule compounds TazTCz, PhTazDCz and DPhTazCz were successfully synthesized and applied as host materials in blue PHOELDs. According to the measurement and quantum chemical calculation, replacing carbazolyl by phenyl enhances the molecular planarity and conjugation degree resulting in the red-shifted emission peaks and the improvement of the fluorescence quantum yield. The compounds have high triplet state energies ~2.86 eV indicating that they can be applied as host materials for blue PHOLEDs. TOF measurement confirms the bipolar transporting properties of these compounds. X-ray single crystal structural analysis demonstrated the propeller-shaped structure of TazTCz, which prevented the intermolecular stacking. The PHOLED with PhTazDCz as host exhibits the lowest turn-on voltage at 2.78 V and slightly efficiency roll-off at high current density because of the balanced carrier mobilities of PhTazDCz.

Acknowledgments We acknowledge the financial support from National Natural Science Foundation of China (21176180) and Specialized Research Fund for the Doctoral Program of Higher Education (20130032110026).

References

1. S. Chen, L. Deng, J. Xie, L. Peng, L. Xie, Q. Fan, W. Huang, Adv. Mater. **22**, 5227–5239 (2010)
2. D.K. Flattery, C.R. Fincher, D.L. LeCloux, M.B. O'Regan, J.S. Richard, Inf. Disp. **27**, 8–13 (2011)
3. P.A. Levermore, V. Adamovich, K. Rajan, W. Yeager, C. Lin, S. Xia, G.S. Kottas, M.S. Weaver, R. Kwong, R. Ma, M. Hack, J.J. Brown, SID Symp. Dig. Tech. Pap. **41**, 786–789 (2010)
4. J.W. Park, D.C. Shin, S.H. Park, Semicond. Sci. Technol. **26**, 034002 (2011)
5. M. Segal, M.A. Baldo, R.J. Holmes, S.R. Forrest, Z.G. Soos, Phys. Rev. B. **68**, 075211 (2003)
6. C. Adachi, M.A. Baldo, M.E. Thompson, S.R. Forrest, J. Appl. Phys. **90**, 5048–5051 (2001)
7. L. Zeng, T.Y.H. Lee, P.B. Merkel, S.H. Chen, J. Mater. Chem. **19**, 8772–8781 (2009)
8. Q. Li, L.S. Cui, C. Zhong, X.D. Yuan, S.C. Dong, Z.Q. Jiang, L.S. Liao, Dyes Pigments **101**, 142–149 (2014)
9. H.Y. Wang, G. Chen, X.P. Xu, S.J. Ji, Aust. J. Chem. **63**, 712–718 (2010)
10. J.W. Kang, S.H. Lee, H.D. Park, W.I. Jeong, K.M. Yoo, Y.S. Park, J.J. Kim, Appl. Phys. Lett. **90**, 223508 (2007)
11. M.H. Tsai, Y.H. Hong, C.H. Chang, H.C. Su, C.C. Wu, A. Matoliukstyte, J. Simokaitiene, S. Grigalevicius, J.V. Grazulevicius, C.P. Hsu, Adv. Mater. **19**, 862–866 (2007)
12. B. Zhang, G. Tan, C. Lam, B. Yao, C.L. Ho, L. Liu, Z. Xie, W.Y. Wong, J. Ding, L. Wang, Adv. Mater. **24**, 1873–1877 (2012)
13. M.H. Ho, B. Balaganesan, T.Y. Chu, T.M. Chen, C.H. Chen, Thin Solid Films **517**, 943–947 (2008)
14. R.A. Klenkler, H. Aziz, A. Tran, Z.D. Popovic, G. Xu, Org. Electron. **9**, 285–290 (2008)
15. H.F. Chen, S.J. Yang, Z.H. Tsai, W.Y. Hung, T.C. Wang, K.T. Wong, J. Mater. Chem. **19**, 8112–8118 (2009)
16. W.Y. Hung, T.H. Ke, Y.T. Lin, C.C. Wu, T.H. Hung, T.C. Chao, K.T. Wong, C.I. Wu, Appl. Phys. Lett. **88**, 064102 (2006)
17. B.R. Kaafarani, A.O. El-Ballouli, R. Trattnig, A. Fonari, S. Sax, B. Wex, C. Risko, R.S. Khnayzer, S. Barlow, D. Patra, T.V. Timofeeva, E.J.W. List, J.L. Brédase, S.R. Mardere, J. Mater. Chem. C **1**, 1638–1650 (2013)

18. G.J. Inzelt, Solid State Electrochem. **7**, 503–510 (2003)
19. Y. Tao, S. Gong, Q. Wang, C. Zhong, C. Yang, J. Qin, D. Ma, Phys. Chem. Chem. Phys. **12**, 2438–2442 (2010)
20. G.M. Sheldrick, Acta Cryst. **A64**, 112–122 (2008)
21. O.V. Dolomanov, L.J. Bourhis, R.J. Gildea, J.A.K. Howardand, H. Puschmann, J. Appl. Cryst. **42**, 339–341 (2009)
22. M.J. Frisch, G.W. Trucks, H.B. Schlegel, G.E. Scuseria, M.A. Robb, J.R. Cheeseman, *Gaussian 03. Revision E. 01* (Gaussian Inc., Wallingford, 2004)
23. P. Moonsin, N. Prachumrak, R. Rattanawan, T. Keawin, S. Jungsuttiwong, T. Sudyoadsuk, V. Promarak, Chem. Commun. **48**, 3382–3384 (2012)
24. J. Li, R. Liu, Z. Zhao, Z. Zhou, J. Mater. Sci.: Mater. Electron. **25**, 1970–1975 (2014)
25. P.M. Borsenberger, J.J. Fitzgerald, J. Phys. Chem. **97**, 4815–4819 (1993)